An S-Shaped Double Helicene Showing both Multi-Resonance Thermally Activated Delayed Fluorescence and Circularly Polarized Luminescence

John Marques dos Santos,[a] Dianming Sun,[a] Juan Manuel Moreno Naranjo,[b] David Hall,[a,c] Francesco Zinna,[d] Seán T. J. Ryan,[b] Wenda Shi,[b] Tomas Matulaitis,[a] David B. Cordes,[a] Alexandra M. Z. Slawin,[a] David Beljonne,[c] Stuart L. Warriner,[e] Yoann Olivier,[f]* Matthew J. Fuchter[b]* and Eli Zysman-Colman[a]*

[a]Organic Semiconductor Centre, EaStCHEM School of Chemistry, University of St Andrews, St Andrews, KY16 9ST, UK. E-mail: eli.zysman-colman@st-andrews.ac.uk;

[b]Department of Chemistry, Molecular Sciences Research Hub, Imperial College London, White City Campus, London, W12 0BZ, UK. Email: m.fuchter@imperial.ac.uk

[c]Laboratory for Chemistry of Novel Materials, University of Mons, 7000 Mons, Belgium.

[d]Dipartimento di Chimica e Chimica Industriale, Università di Pisa, 56124 Pisa, Italy

[e] School of Chemistry, University of Leeds, Leeds, LS2 9JT, UK

[f]Laboratory for Computational Modeling of Functional Materials, Namur Institute of Structured Matter, Université de Namur, Rue de Bruxelles, 61, 5000 Namur, Belgium. E-mail: yoann.olivier@unamur.be
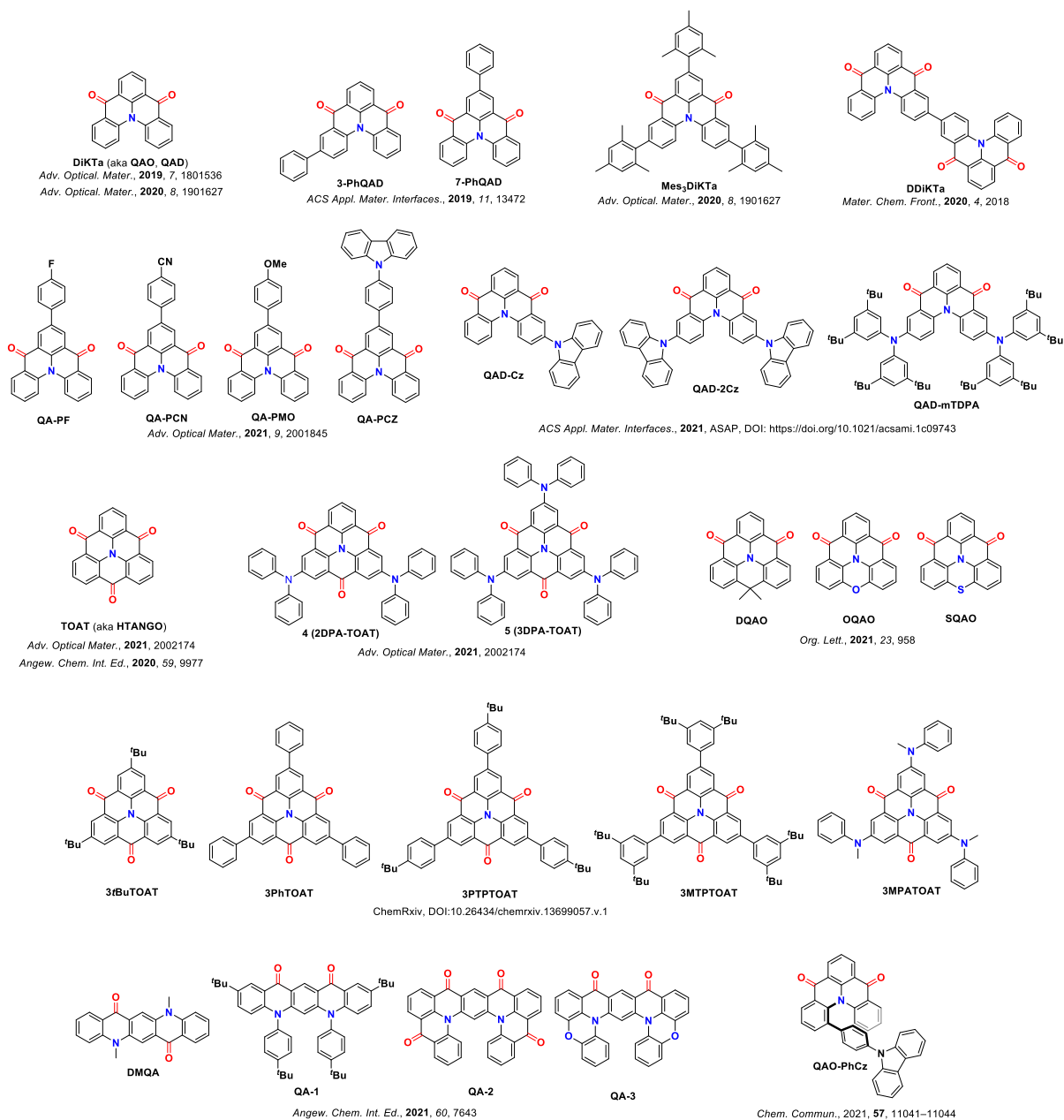
## **Electronic Supporting Information**

Figure S1. Chemical structures of prior examples of N/CO MR-TADF emitters.[1,2,11,12,3–10]

1. Experimental Section

General Synthetic Procedures. All reagents and solvents were obtained from commercial sources and used as received. Air-sensitive reactions were performed under a nitrogen atmosphere using Schlenk techniques, no special precautions were taken to exclude air or moisture during work-up. DCM was obtained from a MBraun SPS5 solvent purification system. Flash column chromatography was carried out using silica gel (Silia-P from Silicycle, 60 Å, 40-63 µm). Analytical thin-layer-chromatography (TLC) was performed with silica plates with aluminum backings (250 µm with F-254 indicator). TLC visualization was accomplished by 254/365 nm UV lamp. HPLC analysis was conducted on a Shimadzu LC-40 HPLC equipped with a Shim-pack GIST 3µm C18 reverse phase analytical column. GCMS analysis was conducted using a Shimadzu QP2010SE GC-MS equipped with a Shimadzu SH-Rtx-1 column (30 m × 0.25 mm). ^{1}H and ^{13}C NMR spectra were recorded on a Bruker Advance spectrometer (400 MHz for ^{1}H and either 101 or 126 MHz for ^{13}C). The following abbreviations have been used for multiplicity assignments: "s" for singlet, "d" for doublet, "t" for triplet, "m" for multiplet, and "dd" for doublet of doublets. ^{1}H and ^{13}C NMR spectra were referenced residual solvent peaks with respect to TMS (δ = 0 ppm). Melting points were measured using open-ended capillaries on an Electrothermal 1101D Mel-Temp apparatus and are uncorrected. High-resolution mass spectrometry (HRMS) was performed in the School of Chemistry of the University of Leeds.

2. Synthetic procedures and characterization data

Tetramethyl 2,2',2'',2'''-(1,3-phenylenebis(azanetriyl))tetrabenzoate (1):
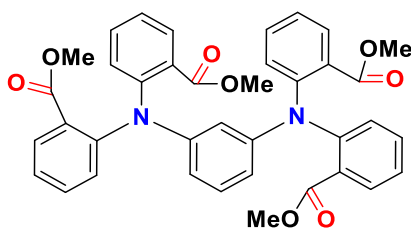
A 2-neck flask held under nitrogen was charged with benzene-1,3-diamine (2.66 g, 24.6 mmol, 1 equiv.), methyl 2-iodobenzoate (38.7 g, 21.7 mL, 148 mmol, 6 equiv.), copper (929 mg, 14.8

mmol, 0.6 equiv.), copper(I) iodide (656 mg, 3.44 mmol. 0.14 equiv.), anhydrous potassium carbonate (20.4 g, 148 mmol, 6 equiv.), and 50 mL anhydrous di-n-butyl ether. The resulting reaction mixture was heated to reflux and stirred for 48 hours. After cooling to room temperature, the mixture was filtered through a pad of celite. The filtrate was then mixed with dichloromethane (50 mL) and washed with water (3 × 50 mL). The organic layer was then dried over anhydrous sodium sulfate and concentrated under reduced pressure. The resulting dark brown oil was purified by column chromatography on silica gel (EtOAc : hexanes = 20 : 80). The corresponding fractions were collected and evaporated under reduced pressure to afford the desired product as a brown reddish solid (8.80 g, 55%). **R$_f$**: 0.10 (EtOAc : hexane = 20 : 80). Mp: 170–172 °C. **^{1}H NMR** (400 MHz, DMSO-d_6) δ 7.46 (m, 8H), 7.13 (t, J = 7.5 Hz, 4H), 7.07–6.99 (m, 5H), 6.31 (dd, J = 8.1, 2.2 Hz, 2H), 6.15 (t, J = 2.2 Hz, 1H), 3.38 (s, 12H). **^{13}C NMR** (101 MHz, DMSO-d_6) δ 167, 149, 145, 132, 130, 129, 128, 127, 124, 115, 115, 52. **HR-MS [M+H]$^+$** Calculated: 645.2237 ($C_{38}H_{33}N_2O_8$); Found: 645.2221.

Diacridino[10,4-ab:10',4'-ij][1,7]phenanthroline-6,10,18,22-tetraone (Hel-DiDiKTa):
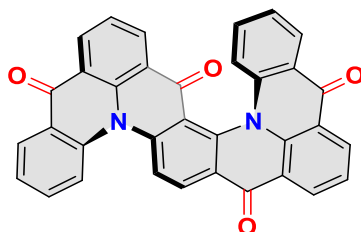
Compound **1** (5.0 g, 7.8 mmol, 1 equiv.) was combined with sodium hydroxide (3.1 g, 78 mmol, 10 equiv.) in 100 mL of an ethanol/water (1:1) mixture. The reaction was heated to reflux for 12 h. After cooling to room temperature, the pH was adjusted to 2-3 by addition of dilute hydrochloric acid. The tetra-acid precipitated as a brown greenish solid and was collected by vacuum filtration, washed thoroughly with water, dried under vacuum (4.52 g, 99% yield) and used without further purification and characterization. The tetra-acid (2.5 g, 4.25 mmol, 1 equiv.) was dispersed in 60 mL dichloromethane under a nitrogen atmosphere. To the reaction mixture were added sequentially thionyl chloride (20.2 g, 12.3 mL, 170 mmol, 40 equiv.) and 6 drops of N,N-dimethylformamide. After 3 h under reflux, the reaction mixture was cooled to room temperature. Under a positive flow of nitrogen, aluminium chloride (11.3 g, 85.0 mmol, 20 equiv.) was added slowly with stirring (exothermic reaction). After refluxing for 24 h, the

reaction mixture was cooled to room temperature, and the reaction quenched by slow dropwise of water under vigorous stirring (exothermic reaction). The resulting mixture was combined with more dichloromethane (50 mL), the organic layer separated and washed with water (3 × 50 mL), and then dried over anhydrous sodium sulfate. The solvent was evaporated under reduced pressure and the brown solid crude product was purified by column chromatography on silica gel (CH$_2$Cl$_2$:EtOAc = 7:3) to yield (*rac*)-**Hel-DiDiKTa** as an orange solid (0.79 g, 36%). **R$_f$**: 0.60 (CH$_2$Cl$_2$:EtOAc = 7:3). **Mp**: > 390 °C. **^{1}H NMR** (400 MHz, DMSO-*d$_6$*) δ 8.71– 8.50 (m, 5H), 8.37 (d, *J* = 7.9 Hz, 2H), 8.26 (m, 3H), 7.94 (t, *J* = 7.7 Hz, 1H), 7.81 (t, *J* = 7.6 Hz, 1H), 7.67 (t, *J* = 7.4 Hz, 2H), 7.46– 8.50 (m, 2H). **^{13}C NMR** (126 MHz, DMSO-*d$_6$*) δ 179, 176, 139, 139, 133, 132, 132, 130, 127, 126, 126, 125, 125, 123, 123, 122. **Anal. Found**: C, 78.18%; H, 3.14%; N, 5.21. **Anal. Calcd. For C$_{34}$H$_{16}$N$_2$O$_4$**: C, 79.06%; H, 3.12%; N, 5.42%. **HR-MS [M+H]$^+$** Calculated: 517.1188 (C$_{34}$H$_{17}$N$_2$O$_4$); Found: 517.1177. 99.1 % pure on HPLC analysis, retention time 31.3 minutes in 60% methanol 40% water.
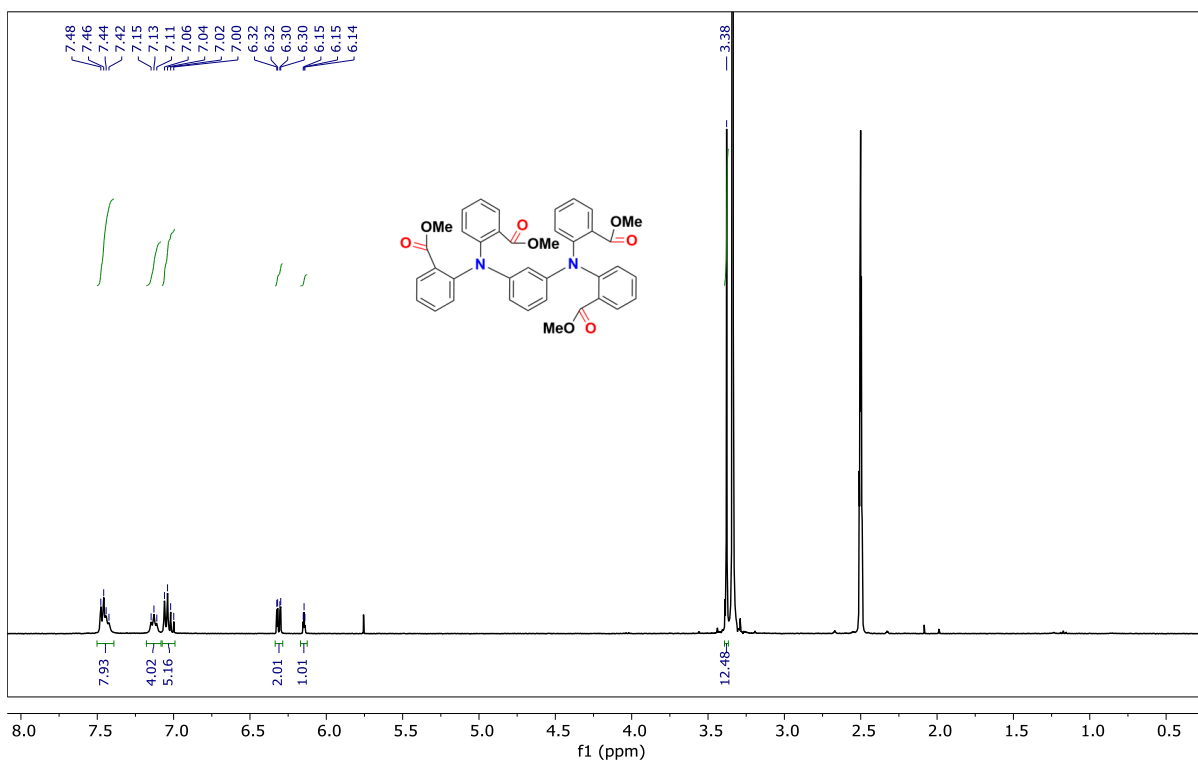
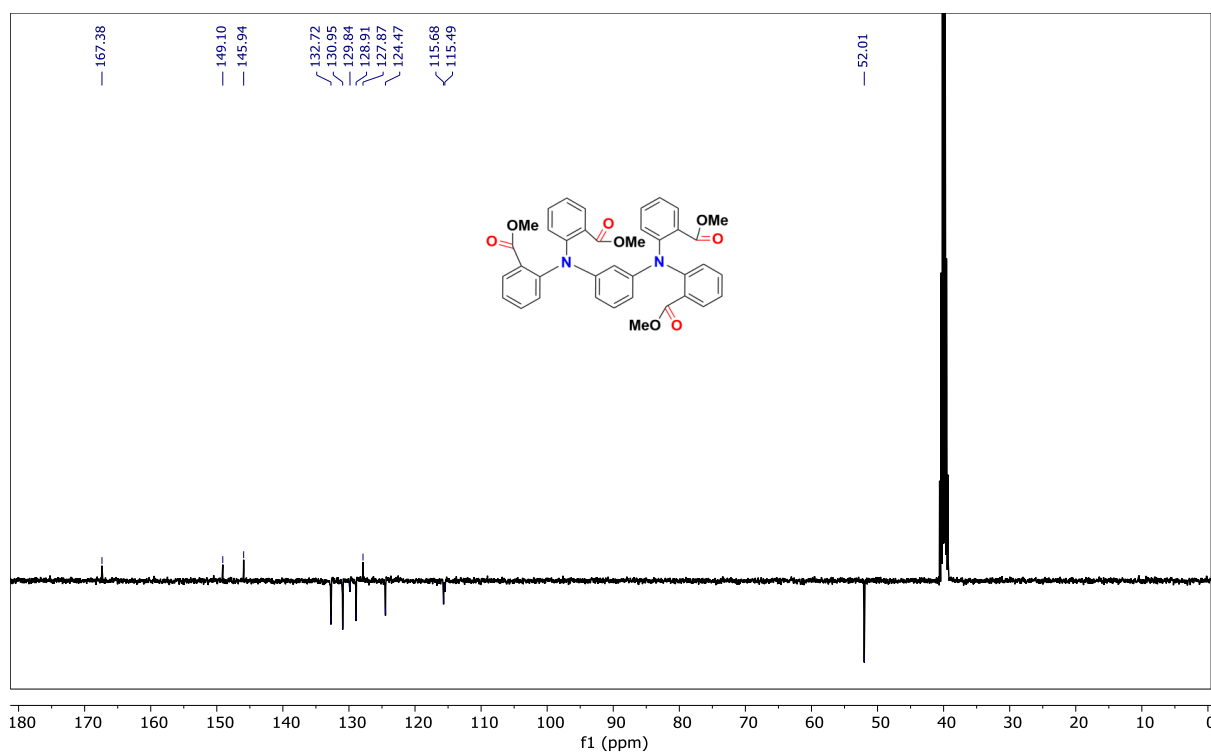**Figure S2**. ^{1}H NMR (400 MHz, DMSO-d_6) of compound **1**.
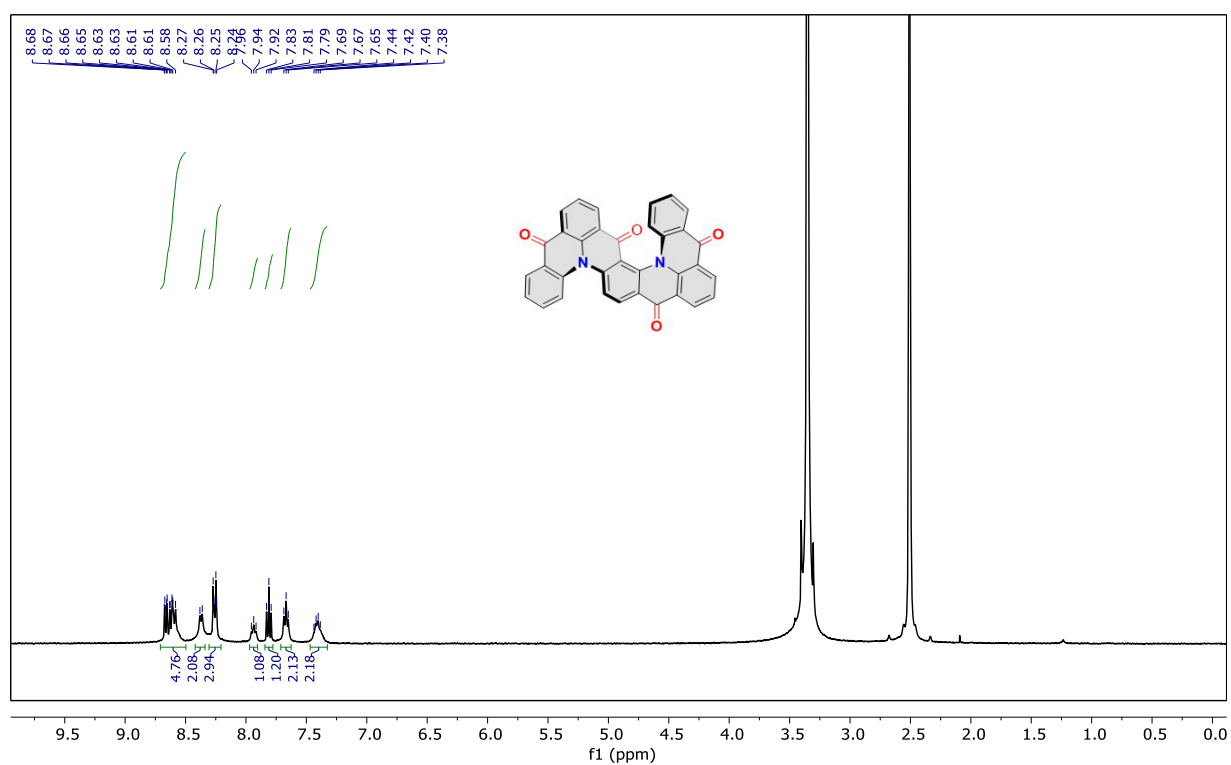

Figure S3. DEPTq (101 MHz, DMSO-d_6) of compound **1**.

Figure S4. ¹H NMR (400 MHz, DMSO-*d*₆) of (*rac*)-**Hel-DiDiKTa**.
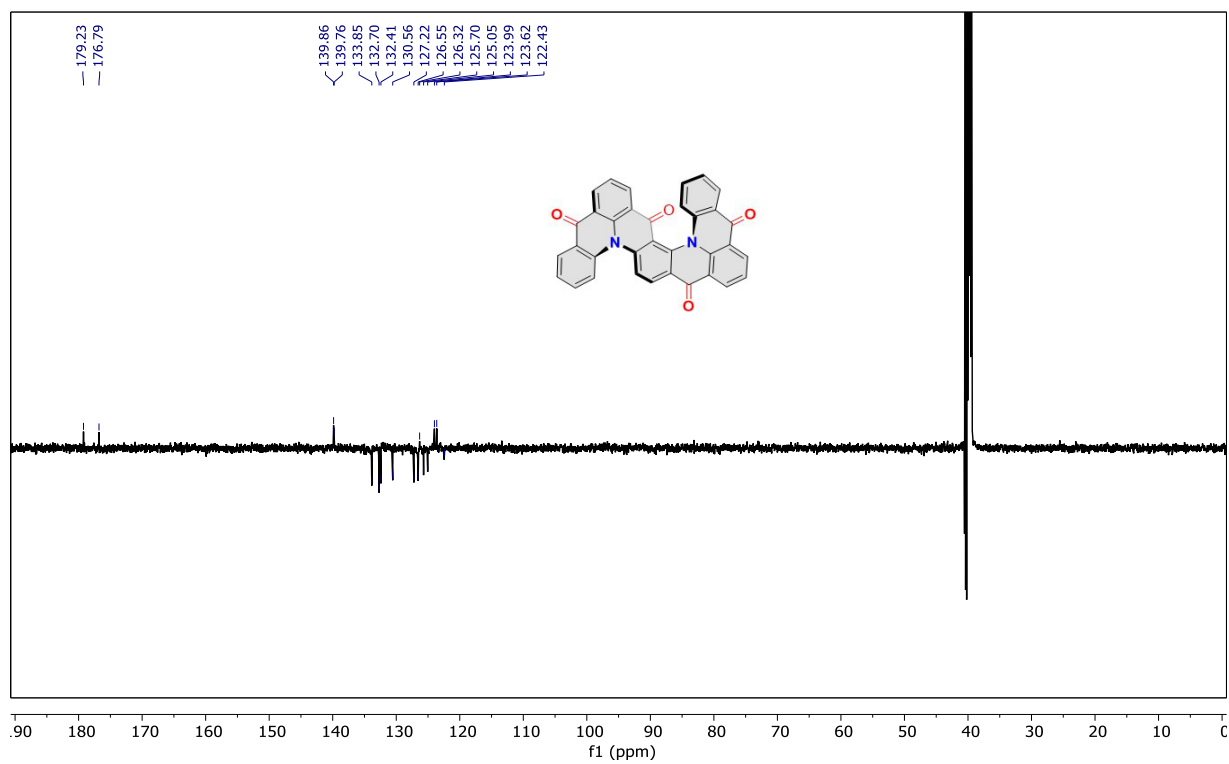

Figure S5. DEPTq (126 MHz, DMSO-*d*₆) of (*rac*)-**Hel-DiDiKTa**.
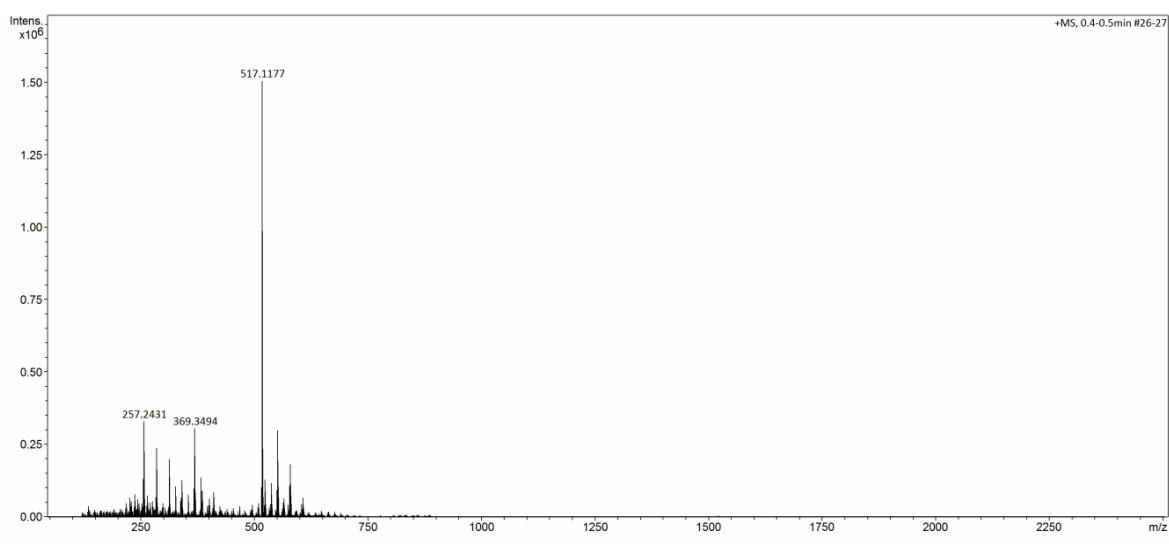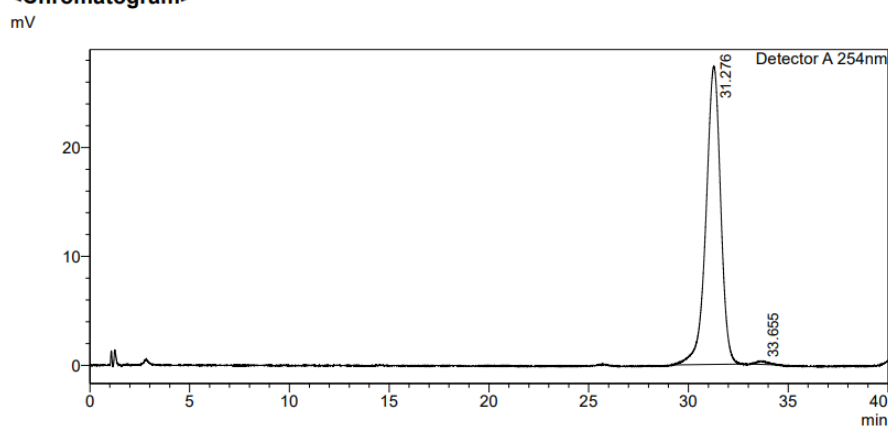
Figure S6. HRMS of (*rac*)-**Hel-DiDiKTa**.

<Sample Information>

Sample Name   : JMDS_012_Run2
Sample ID   :
Method Filename : 60% Methanol 40 Water 40 mins.lcm
Batch Filename   : JMDS_012_Unsublimated.lcb
Vial #   : 1-20   Sample Type   : Unknown
Injection Volume : 10 uL
Date Acquired   : 06/01/2021 14:17:29   Acquired by   : System Administrator
Date Processed   : 06/01/2021 14:57:29   Processed by   : System Administrator

<Chromatogram>

<Peak Table>

Detector A 254nm

Peak#	Ret. Time	Area	Height	Area%	Area/Height	Width at 5% Height
1	31.276	1399557	27357	99.139	51.158	1.808
2	33.655	12156	277	0.861	43.946	1.259
Total		1411713	27634	100.000		

Figure S7. HPLC trace of (*rac*)-**Hel-DiDiKTa**.

3. X-Ray Crystallography

X-ray diffraction data for (*rac*)-**Hel-DiDiKTa** were collected at 173 K using a Rigaku MM-007HF High Brilliance RA generator/confocal optics with XtaLAB P100 diffractometer [Cu Kα radiation (λ = 1.54187 Å)]. Intensity data were collected using both ω and φ steps accumulating area detector images spanning at least a hemisphere of reciprocal space. Data for all compounds analysed were collected using CrystalClear[13] and processed (including correction for Lorentz, polarization and absorption) using CrysAlisPro.[14] The structure was solved by dual-space methods (SHELXT[15]) and refined by full-matrix least-squares against F^2 (SHELXL-2018/3[16]). Non-hydrogen atoms were refined anisotropically, and hydrogen atoms were refined using a riding model. All calculations were performed using the Olex2[17] interface. Deposition number 2105660 contains the supplementary crystallographic data for this paper. These data are provided free of charge by the joint Cambridge Crystallographic Data Centre and Fachinformationszentrum Karlsruhe Access Structures service www.ccdc.cam.ac.uk/structures.

Crystal data for (*rac*)-**Hel-DiDiKTa**. $C_{34}H_{16}N_2O_4$, $M = 516.49$, orthorhombic, $a = 14.2194(2)$, $b = 14.4571(2)$, $c = 21.6864(3)$ Å, $U = 4458.10(11)$ Å^3, $T = 173$ K, space group *Pbca* (no. 61), $Z = 8$, 45132 reflections measured, 4079 unique ($R_{int} = 0.0281$), which were used in all calculations. The final R_1 [$I > 2\sigma(I)$] was 0.0399 and wR_2 (all data) was 0.0974.
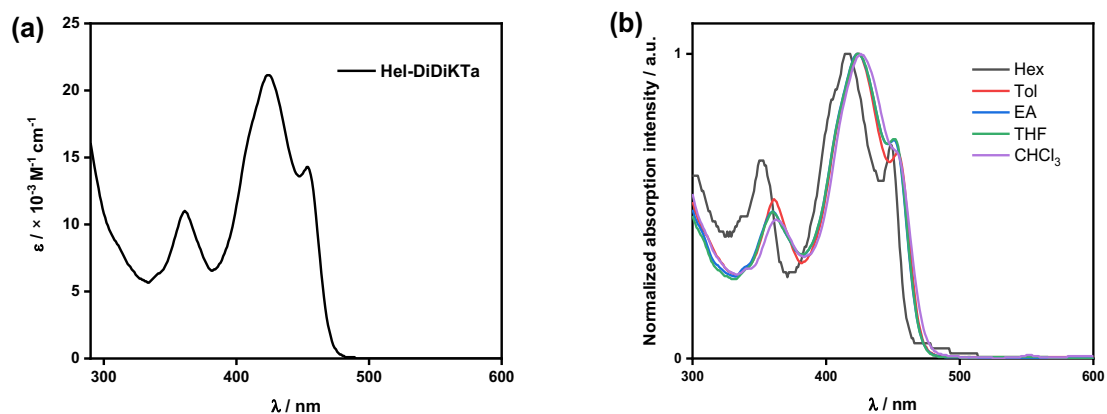
4. Photophysical data

Figure S8. (a) Absorption spectrum of (*rac*)-**Hel-DiDiKTa** obtained in toluene (1.01×10^{-5} M) at 300 K. (b) Solvatochromic absorption study of (*rac*)-**Hel-DiDiKTa**.
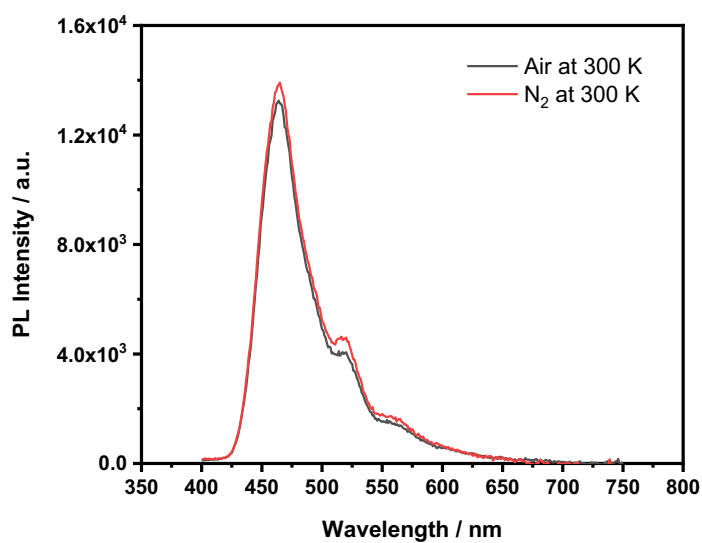

Figure S9. SS PL spectra of (*rac*)-**Hel-DiDiKTa** in toluene obtained in air and under N_2 at 300 K, $\lambda_{exc} = 350$ nm.
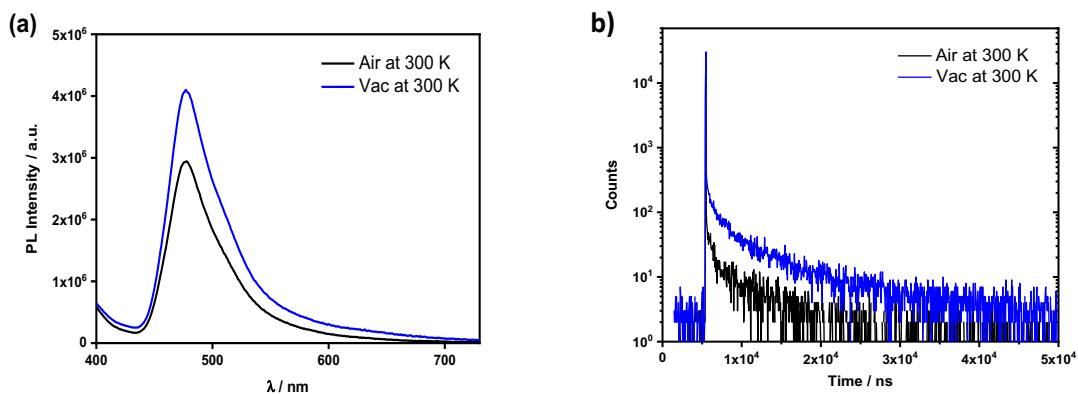
Figure S10. (a) SS PL spectra of (*rac*)-**Hel-DiDiKTa** in mCP in air and under vacuum at 300 K, λ_{exc} = 350 nm. (b) Time-resolved PL of 1 wt% (*rac*)-**Hel-DiDiKTa** in mCP in air and under vacuum at 300 K, λ_{exc} = 378 nm.

Table S1. Summary of solvatochromic PL properties of (*rac*)-**Hel-DiDiKTa.**

Solvent	λ_{PL} [a]	FWHM [b]
	nm	nm / eV
Hexane (Hex)	452	42 / 0.25
Toluene (Tol)	463	44 / 0.26
Ethyl acetate (EA)	464	50 / 0.28
THF	467	50 / 0.28
CHCl$_3$	470	50 / 0.28

[a] Peak value of PL spectra obtained under aerated conditions at 300 K, concentration 1×10^{-5} M, λ_{exc} = 350 nm. [b] Full width at half maximum of the corresponding PL spectra.

Table S2. PLQY (Φ_{PL}) study of (*rac*)-**Hel-DiDiKTa** at different doping concentration in mCP, λ_{exc} = 350 nm.

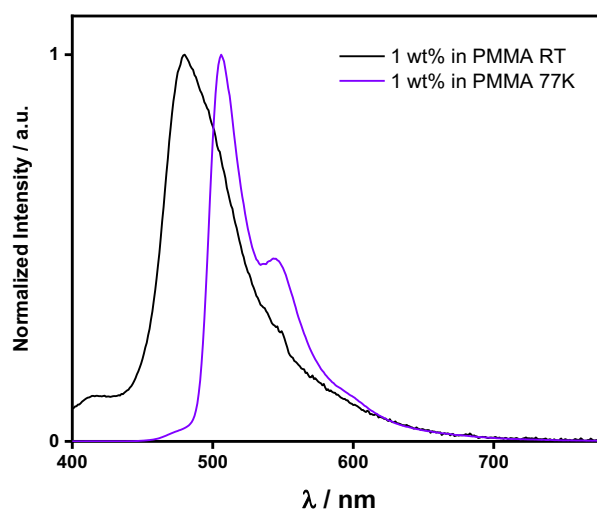| Doping concentration / %	$\Phi_{PL}(N_2)$ / %	$\Phi_{PL}(air)$ / %
3	5	5
10	4	4
30	4	4
50	5	4
Neat film	4	4

Figure S11. Steady state PL spectrum at RT and at 77 K of (*rac*)-**Hel-DiDiKTa** in 1 wt% PMMA. λ_{exc} = 350 nm.
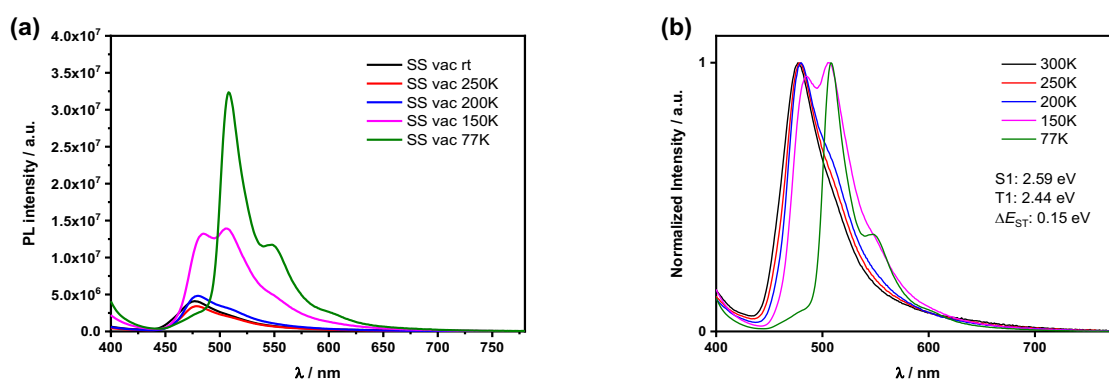

Figure S12. Temperature-dependent PL study of 1 wt% (*rac*)-**Hel-DiDiKTa** in mCP (a) non-normalized spectra, and (b) normalized spectra, λ_{exc} = 350 nm.

Table S3. S_1, T_1 and ΔE_{ST} values of (*rac*)-**Hel-DiDiKTa** obtained from the onsets of the prompt fluorescence and phosphorescence in different media.

a In toluene			b 1 wt% in mCP			c 1 wt% in PMMA		
S_1 / eV	T_1 / eV	ΔE_{ST} / eV	S_1 / eV	T_1 / eV	ΔE_{ST} / eV	S_1 / eV	T_1 / eV	ΔE_{ST} / eV
2.77	2.51	0.26	2.78	2.52	0.26	2.76	2.53	0.23

a) S_1, T_1 and ΔE_{ST} values of (*rac*)-**Hel-DiDiKTa** calculated from the onsets of the prompt fluorescence and phosphorescence spectra in toluene glass at 77 K, b) in 1 wt% (*rac*)-**Hel-DiDiKTa** doped in mCP, c) and in 1 wt% (*rac*)-**Hel-DiDiKTa** doped in PMMA.

Table S4. Temperature-dependent Transient PL decay data of 1 wt% (*rac*)-**Hel-DiDiKTa** doped into mCP matrix.[a]

Temperature	τ_1 / ns	τ_2 / ns	τ_3 / ns	A_1	A_2	A_3	R_1 %	R_2 %	R_3 %
300K	134	1408	7629	322	86	29	11.2	31.5	57.3
250K	75	2196	15985	454	88	63	2.8	15.6	81.7
200K	32	368	24142	1345	97	74	2.3	1.9	95.8
150K	28.6	1565	-	295	4.4	-	55	45	-

a) The transient PL decay data were fitted by triple-exponential function, where A_i is the pre-exponential for lifetime τ_i. R_i is individual component ratio for prompt and delayed fluorescence. $R_i = \tau_i A_i / \Sigma \tau_i A_i$.

Determination of photophysical parameters

The efficiencies (Φ_p and Φ_d) and constants (k_p and k_d) for prompt and delayed emission can be estimated according to their contributions to total Φ_{PL} and their lifetimes (τ_p and τ_d) according to the triple exponential fitting of time-resolved decay curves at 300 K.

To determine the rates, we used the following equations according to previous studies[18] of TADF photophysical processes:

$$\Phi_{ISC} = \frac{\Phi d/\Phi p}{1+\Phi d/\Phi p} \quad (1)$$

$$\Phi_{RISC} = \frac{k_{RISC}}{k_{RISC}+k_{nr}\mathrm{T}} \quad (2)$$

$$k_p = \frac{\Phi p}{\tau_p} \quad (3)$$

$$k_d = \frac{\Phi d}{\tau_d} \quad (4)$$

$$k_r^S = \Phi_p \times k_p \quad (5)$$

$$k_{ISC} = \frac{\Phi ISC}{\tau_p} \quad (6)$$

$$k_{RISC} = \frac{kp \times kd}{kISC} \left(\frac{\Phi d}{\Phi p}\right) \quad (7)$$

$$k_{nr}^T = k_d - (1 - \frac{kISC}{kp}) \times k_{RISC} = k_d - (1 - \frac{kISC}{kp}) \times \frac{kd \times kp \times \Phi d}{kISC \times \Phi p} \quad (8)$$

where Φ_{PL} is the absolute Φ_{PL}; Φ_p and Φ_d are the prompt and delayed fluorescence efficiencies, respectively; k_p and k_d are the prompt and delayed fluorescence decay rate, respectively; τ_p and τ_d are the lifetimes of prompt and delayed fluorescence; nr, ISC and RISC are non-radiative conversion, intersystem crossing and reverse intersystem crossing processes.

Table S5. Photophysical properties of 1 wt% (rac)-**Hel-DiDiKTa** doped into mCP matrix **at 300 K**

Temperature	τ_p [a]	τ_d [b]	k_p [c]	k_d [d]	k_r^S [e]	k_{ISC} [f]	k_{RISC} [g]	k_{nr}^T [h]	Φ_{RISC} [i]
/K	/ ns	/ μs	/ ×10⁴ s⁻¹	/ ×10³ s⁻¹	/ ×10² s⁻¹	/ ×10⁶ s⁻¹	/ ×10² s⁻¹	/ ×10³ s⁻¹	/ %
300	134	5.4	4.2	8.2	2.3	6.6	4.1	8.2	4.5

[a] lifetime of prompt emission; [b] lifetime of delayed emission; [c] decay rate constant of prompt emission; [d] decay rate constant of delayed emission; [e] radiative decay rate constant of singlet excitons; [f] intersystem crossing rate constant; [g] reverse intersystem crossing rate constant; [h] nonradiative decay rate constant of triplet excitons; [i] percentage of reverse intersystem crossing.
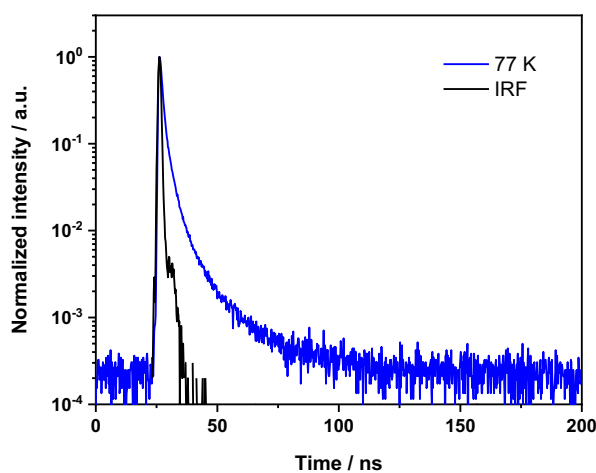

Figure S13. Time-resolved PL of 1 wt% (*rac*)-**Hel-DiDiKTa** in mCP under vacuum at 77 K, λ_{exc} = 378 nm.

Table S6. Electrochemical data of (*rac*)-**Hel-DiDiKTa** compared to the parent **DiKTa**.[2]

Compound	E_{ox} [a] / V	E_{red} [a] / V	HOMO [b] / eV	LUMO [b] / eV	ΔE [c] / eV
(rac)-**Hel-DiDiKTa**	1.81	-1.16	-6.15	-3.18	2.97
DiKTa	1.66[2]	-1.33[2]	-5.93[2]	-3.11[2]	2.82[2]

[a] Potential values obtained for (*rac*)-**Hel-DiDiKTa** from the DPV peak values, measured in degassed dichloromethane with 0.1 M [^{n}Bu$_4$N]PF$_6$ as the supporting electrolyte and referenced with respect to SCE (Fc/Fc$^+$ = 0.46 eV).[19] [b] HOMO and LUMO energy levels determined using the relation $E_{HOMO/LUMO} = -(E_{ox} / E_{red} + 4.8)$ eV (using Fc/Fc$^+$ as the internal reference);[20] [c] $\Delta E = |$ HOMO − LUMO $|$ eV. [2] Value obtained from the literature in MeCN.

*Resolution of (rac)-**Hel-DiDiKTa**.*

Enantiomers were isolated using a Chiralpak IE column (10 mm I.D. x 250 mm) with Toluene:EtOAc 60:40 mobile phase and 5.0 mL min^{-1} flow rate on a recycling HPLC system (Japan Analytical Industry LC-908 HPLC) for 3 cycles and then collected (Figure **S14**). The first enantiomer initially exhibited a retention time of 9.9 min while the second enantiomer exhibited a retention time of 11.5 min. Following separation, the purity of both samples was further checked by cHPLC and UV-Vis absorption, showing high purity for each enantiomer (Figures **S15** and **S16**). Enantiomers exhibited enantiomeric ratios of (e.r.) > 99 % and > 97 % for (*P*) and (*M*) enantiomers, respectively and identical UV-Vis spectra at a concentration ~ 5×10^{-5} M in toluene.
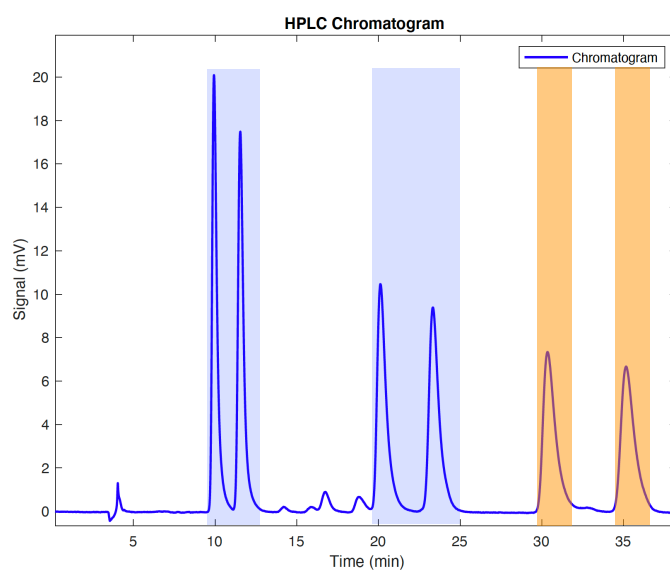
Figure S14. Chiral-HPLC trace of (*rac*)-**Hel-DiDiKTa**. In blue, recycled signals submitted to the next cHPLC cycle. In orange, collected peaks. Both enantiomeric peaks were collected on the third cHPLC cycle.
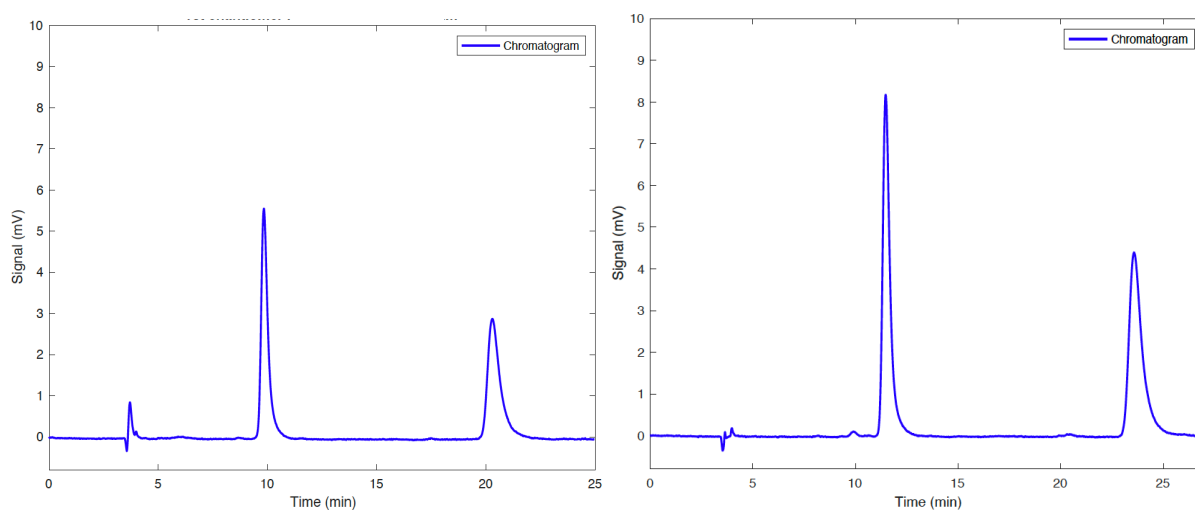

Figure S15. cHPLC traces for (*P*)-**Hel-DiDiKTa** (left) and (*M*)-**Hel-DiDiKTa** (right). After 2 cycles, no significant impurity signals were found.
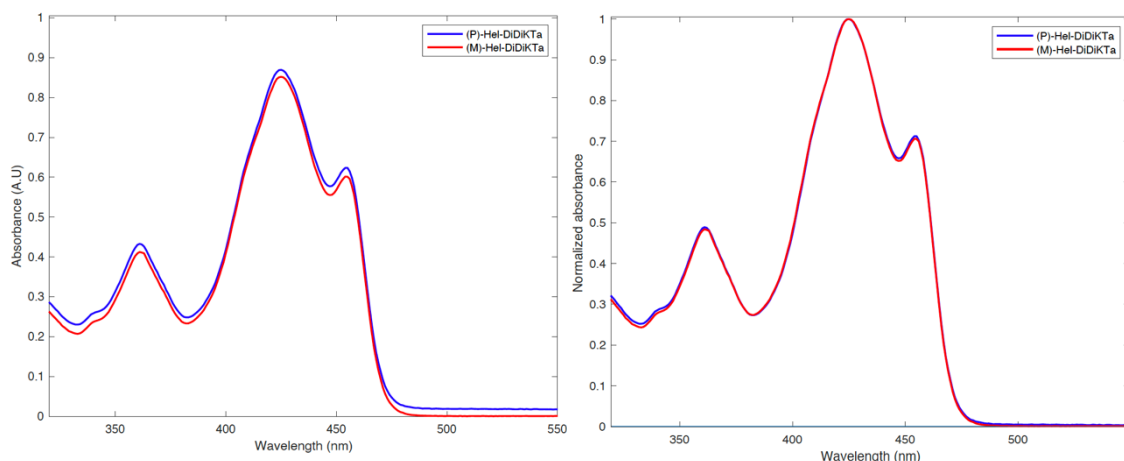
Figure S16. UV-Vis (left) and normalized UV-Vis (right) spectra of (*P*)-**Hel-DiDiKTa** and (*M*)-**Hel-DiDiKTa** in toluene (~5 × 10⁻⁵ M).

Chiroptical spectroscopy

Circular-dichroism spectra were recorded in toluene at a concentration ~2.25 × 10⁻⁵ M (Figure **S17**) using a Chirascan (Applied Photophysics) spectrophotometer. The absorption dissymmetry factors (g_{abs}) values were obtained according to the following equation:

$$g_{abs} = \frac{A_L - A_R}{\frac{1}{2}(A_L + A_R)} \qquad (9)$$

where A_L and A_R represent the magnitude of absorbed left- and right-handed light, respectively. Circularly polarized photoluminescence (CPPL) measurements were performed using a homemade spectrofluoropolarimeter[21] in toluene at a concentration of ~5 × 10⁻⁶ M. The samples were excited by 365 nm radiation (LED source) with a 90° geometry between excitation and detection channels. The excitation light was linearly polarized in the same plane as detection. Parameters used: band width = 10 nm, scan speed = 1 nm sec⁻¹, integration time 4 sec, PMT voltage 700 V, accumulations 10. The g_{PL} factor is fairly constant throughout the emission band (Figure **S18**) and it was quantitatively estimated as the ratio between the integral of CPL spectrum over the integral of total fluorescence.
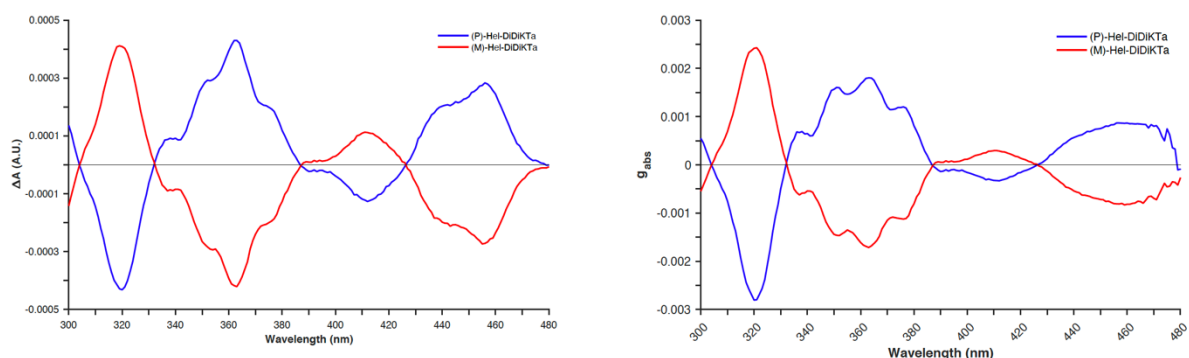
Figure S17. Left: CD spectra. Right: g_{abs} vs. wavelength of (*P*)-**Hel-DiDiKTa** and (*M*)-**Hel-DiDiKTa** in toluene (~2.25 × 10^{-5} M).
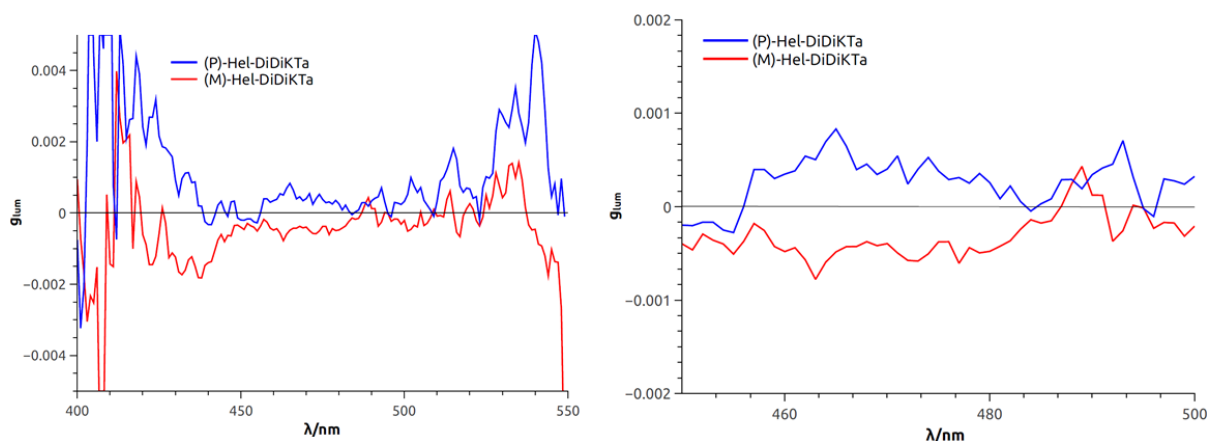

Figure S18. Left: g_{PL} vs. wavelength of (*P*)-**Hel-DiDiKTa** and (*M*)-**Hel-DiDiKTa** in toluene (~5 × 10^{-6} M). Right: an expansion of the 450-500 nm region of the same plot.

Quantum chemical calculations

The calculations were performed with the Gaussian 16 revision A_03[22] suite for the density functional theory (DFT) and with the Turbomole/7.4[23] package for SCS-CC2 calculations. Ground-state optimized structures were calculated using the PBE0 functional[24] and the 6-31G(d,p) basis set in the gas phase.[25] Ground state calculations were also performed with CAM-B3LYP,[26] B3LYP,[27] LCwPBE[28] and M062X[29] functionals at the same basis set. Excited state calculations were performed for each within the Tamm-Dancoff approximation (TDA). Molecular orbitals were visualized using GaussView 5.0 software.[30] Spin-component scaling coupled-cluster singles-and-doubles model (SCS-CC2) was also used in conjunction

with cc-pVDZ basis set.[31] We first optimized the ground state using SCS-CC2 method, then vertical excited states were performed on the ground state optimized structure using the SCS-CC2 method. Difference density plots were used to visualize change in electronic density between the ground and excited state and were visualized using the VESTA package.
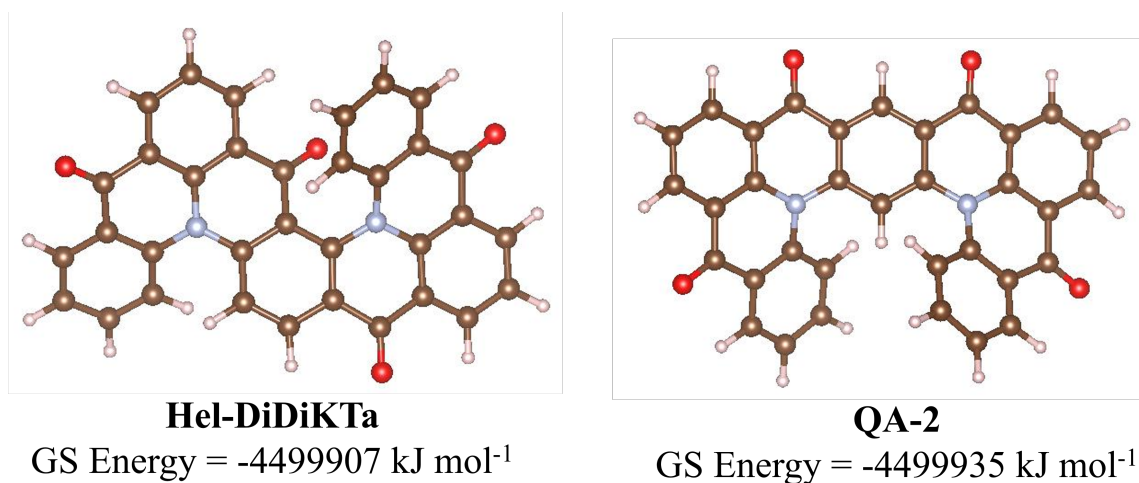

Hel-DiDiKTa
GS Energy = -4499907 kJ mol^{-1}

QA-2
GS Energy = -4499935 kJ mol^{-1}

Figure S19. Ground state energy and pictures of **Hel-DiDiKTa** and **QA-2** calculated at PBE0/6-31 G(d,p).

Table S7. Overall energy of **QA-2** and **Hel-DiDiKTa** in the gas phase using various methods, DFT used 6-31G(d,p) and SCS-CC2 used cc-pVDZ basis set.

Method	**QA-2** energy / kJ mol^{-1}	**Hel-DiDiKTa** energy / kJ mol^{-1}	Δ_{energy} / kJ mol^{-1} [a]
CAMB3LYP	-4502671	-4502642	-29
LCωPBE	-4501739	-4501714	-25
B3LYP	-4505176	-4505149	-26
PBE0	-4499935	-4499907	-29
M062X	-4503030	-4503003	-27
SCS-CC2	-4491500	-4491482	-18

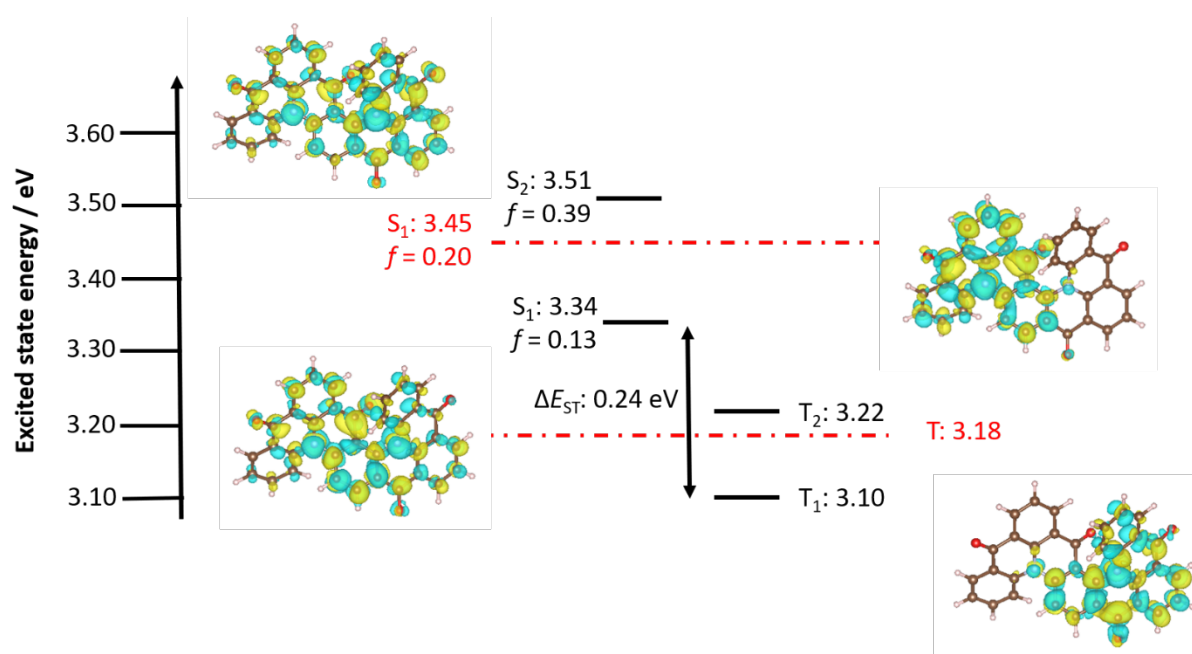[a] (Energy of **QA-2** – Energy of **Hel-DiDiKTa**)

Figure S20. Double electronic excited state difference density plot of **Hel-DiDiKTa** and vertical excited state energies of it and the parent **DiKTa** (dashed red line).

Table S8. Computational data calculated in the gas phase for **Hel-DiDiKTa**, **DiKTa** and previously mentioned CPL-active triangulene, **Hel-DiKTa-2**.[32]

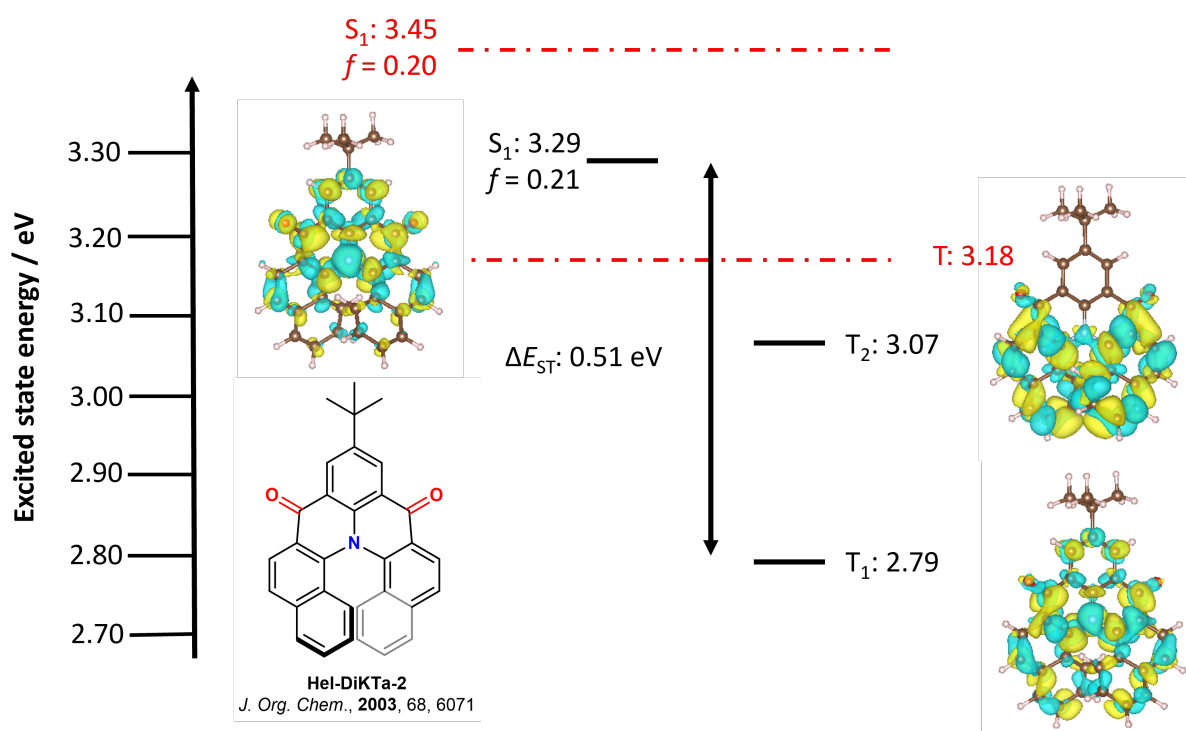| Compound	HOMO / eV	LUMO / eV	ΔE / eV	S_1 / eV (f)	T_1 / eV	T_2 / eV	ΔE_{ST} / eV
DiKTa	-6.20	-2.23	3.97	3.45 (0.20)	3.18	3.60	0.27
Hel-DiDiKTa	-6.26	-2.53	3.73	3.34 (0.13)	3.10	3.22	0.24
Hel-DiKTa-2	-5.90	-2.24	3.66	3.29 (0.21)	2.79	3.07	0.51

Figure S21. Double electronic excited state difference density plot of **Hel-DiKTa-2** and vertical excited state energies of it and the parent **DiKTa** (in dashed red lines).
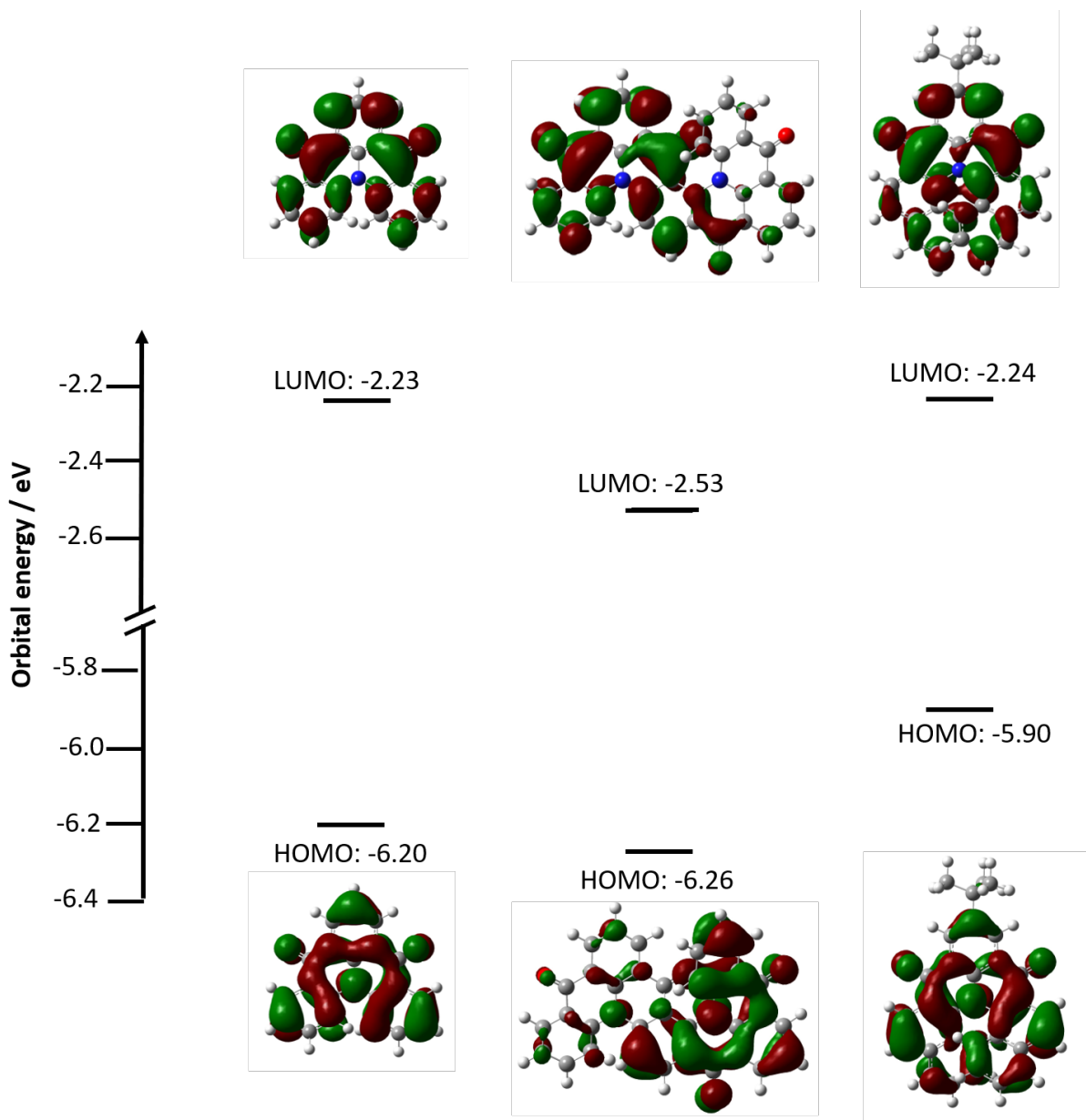
Figure S22. HOMO/LUMO electron density pictures and energies of the **DiKTa**, **Hel-DiDiKTa** and **Hel-DikTa-2** in the gas phase calculated with PBE0/6-31g(d,p), isovalue = 0.02.
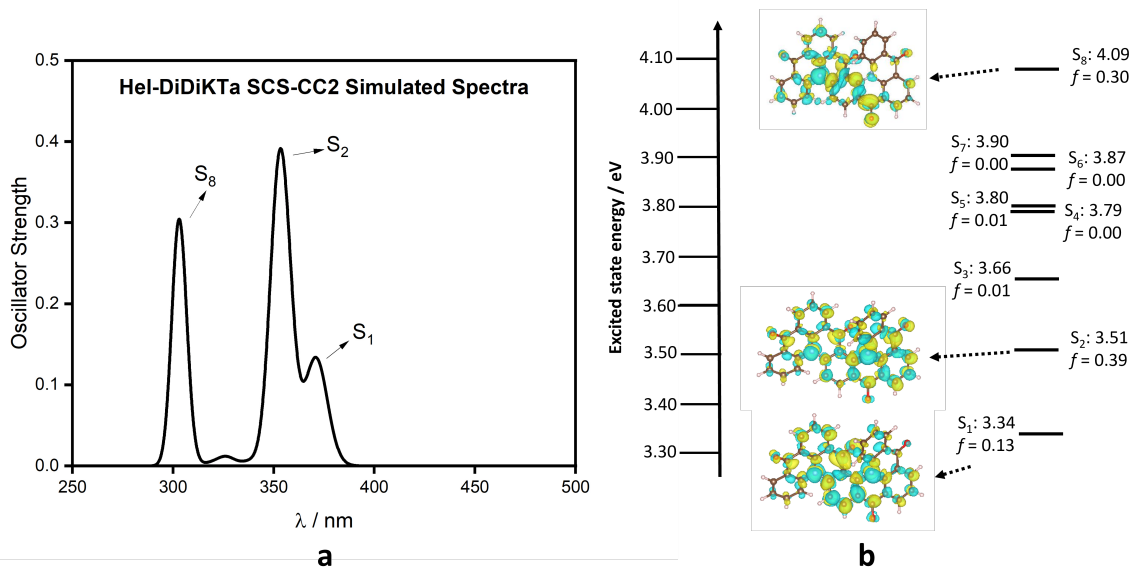
Figure S23. Simulated absorption spectra of **Hel-DiDiKTa** considering first 8 singlet excited states (**a**) and orbital levels of calculated singlet states and relevant important difference density plots (**b**), calculated at SCS-CC2/cc-pVDZ.
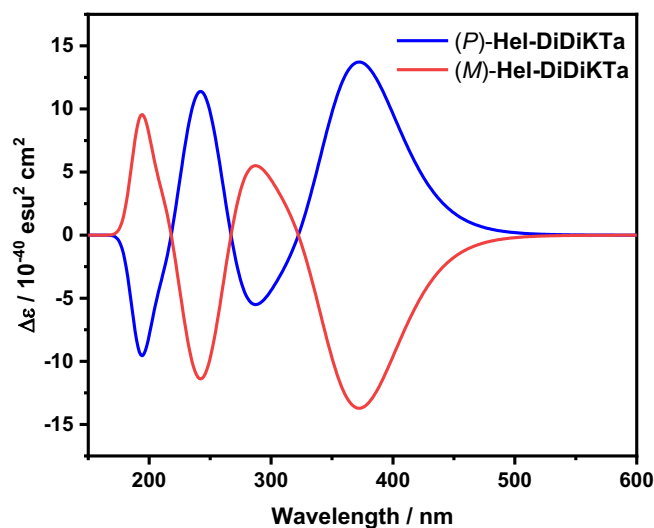

Figure S24. Theoretically simulated CD spectra of (***P***)-**Hel-DiDiKTa** and (***M***)-**Hel-DiDiKTa** calculated in the gas phase calculated at the TDA-DFT/PBE0/6-31g(d,p) from the first 100 singlet excited states. .

Table S9. Chiroptical properties of (***P***)-**HelDiDiKTa** obtained from DFT calculation.

ETDM or μ / 10^{-20} esu·cm				MTDM or m / 10^{-20} erg·G^{-1}				cos θ	θ (deg)	g$_{PL}$
μ_X	μ_Y	μ_Z	$|\mu|$	m_X	m_Y	m_Z	$|m|$			
230.54284	0.81392	44.56212	234.811511	-0.02262856	-0.098583	0.3336785	0.348671679	0.116918	83.28573	6.94 × 10^{-4}

The chriroptical properties were obtained following the method reported in [33], upon optimization of the molecular structure at the lowest-energy singlet excited state (S_1) at the PBE0/6-31g(d,p) level of theory in the gas phase. electric transition dipole moment (ETDM or μ); magnetic transition dipole moment (MTDM or m); θ is the angle between μ and and m.

Enantiomerisation study

After the resolution of both enantiomers, the enantiomerisation process was studied. The CD signal decay from (**P**)-**HelDiDiKTa** dissolved in *p*-xylene at different temperatures (T= 75 ºC, 80 ºC, 85 ºC and 90 ºC) was monitored over time (t) (at 363 nm). CD measurements were carried out using a Chirascan V100 (Applied Photophysics).

For clarity, we refer to 'enantiomerisation' as the molecular process leading to the conversion of one chiral molecule into its opposite chirality counterpart.[34,35] In comparison, 'racemisation' is the macromolecular process by which one sample loses the enantiomeric excess over time due to enantiomerisation. Considering first order kinetics, the following equation describes the process for the enantiomerisation:

$$\ln[A]_t = -k_{rac}t + \ln[A]_o \qquad (10)$$

where $[A]_t$ refers to the concentration of the enantiomer A at a given time, k_{rac} refers to the racemisation constant at a given temperature, t refers to the time and $[A]_o$ refers to the initial concentration of enantiomer A at t=0.[34] Since the value $[A]_t$ is completely analogous to the circular dichroism signal at any given time, we can define the following equation:

$$\ln(\Delta A)_t = -k_{rac}t + \ln(\Delta A)_o \qquad (11)$$

Thus, a linear fit of the natural log of the CD signal against the time results in the racemisation constant from the slope of the fit. By performing this analysis for the results obtained at each of the different temperatures, it is possible to obtain the racemisation constants at each temperature (Figures S24-S27).
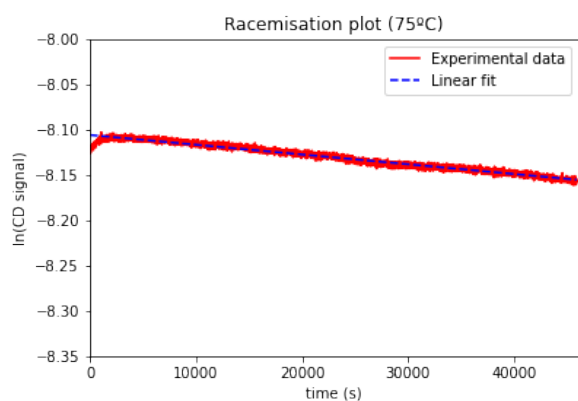
Figure S25. Racemisation plot at 75 ºC.

Slope	Intercept	R^2
$(-1.075\pm0.002)*10^{-6}$ s^{-1}	(-8.10619 ± 0.00006)	0.967
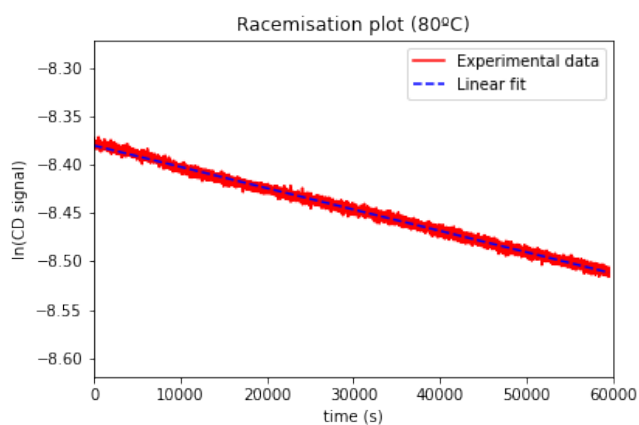
Figure S16. Racemisation plot at 8 0ºC.

Slope	Intercept	R^2
$(-2.214\pm0.002)*10^{-6}$ s^{-1}	(-8.37972 ± 0.00006)	0.993
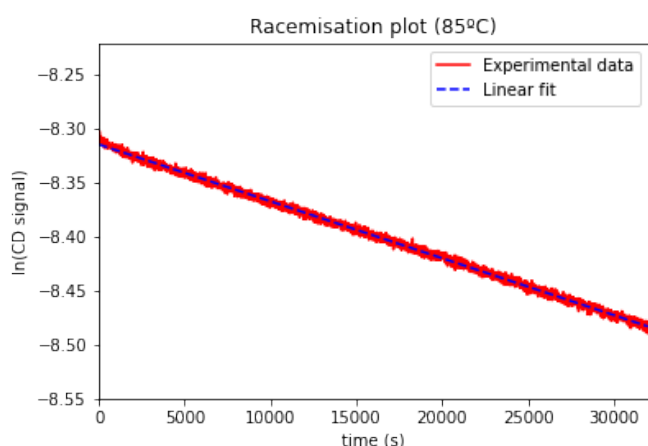
Figure S27. Racemisation plot at 85 ºC.

Slope	Intercept	R^2
$(-5.270\pm0.004)*10^{-6}$ s^{-1}	(-8.31418 ± 0.00007)	0.997
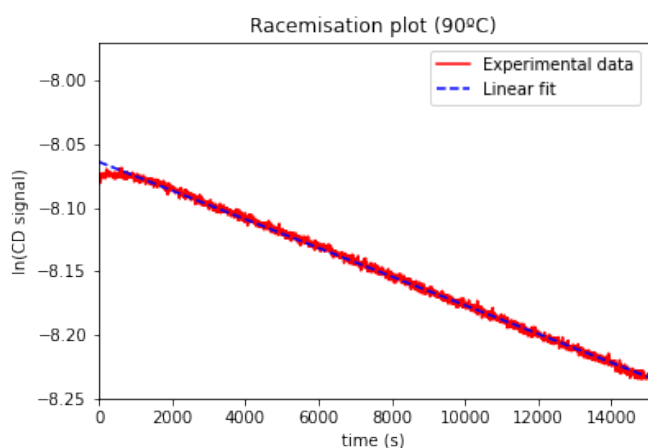
Figure S28, Racemisation plot at 90 ºC.

Slope	Intercept	R^2
$(-1.125\pm0.001)*10^{-5}$ s^{-1}	(-8.0641 ± 0.0001)	0.998

Once all the different racemisation constants have been obtained, an Eyring plot can be used to extract the thermodynamic parameters governing the process i.e., activation enthalpy ($\Delta H_e^{\ddagger}$) and activation entropy ($\Delta S_e^{\ddagger}$) for enantiomerisation (see equation 12). By plotting $\ln(k_e/T)$ vs. $1/T$, a line with slope $a = -(\Delta H_e^{\ddagger}/R)$ and y-intercept $b = (\Delta S_e^{\ddagger}/R + \ln(\kappa\, k_B/h))$ is obtained. [34]

$$\ln\left(\frac{k_e}{T}\right) = -\left(\frac{\Delta H_e^{\ddagger}}{RT}\right) + \frac{\Delta S_e^{\ddagger}}{R} + \ln\left(\frac{\kappa\, k_B}{h}\right) \qquad (12)$$

where R is the universal gas constant (R = 8.31446 × 10⁻³ kJ K⁻¹ mol⁻¹), k_B is the Boltzmann constant (1.380662 ×10⁻²³ J K⁻¹), h is Planck's constant, h = 6.626176 × 10⁻³⁴ J s), k_e is the enantiomerisation rate constant, T is the temperature, $\Delta H_e^{\ddagger}$ is the activation enthalpy for the enantiomerisation process, $\Delta S_e^{\ddagger}$ is the activation entropy for the enantiomerisation process and κ is the transmission coefficient. At the transition state, the molecule has an equal probability to be transformed into either of the enantiomers. For this reason, the value of κ is set to 0.5.[35,36]

It is important to note that the enantiomerisation constant is required for the Eyring plot. The racemisation constants previously obtained are easily converted into their enantiomerisation counterparts using equation 13: [34]

$$2k_e = k_{rac} \tag{13}$$

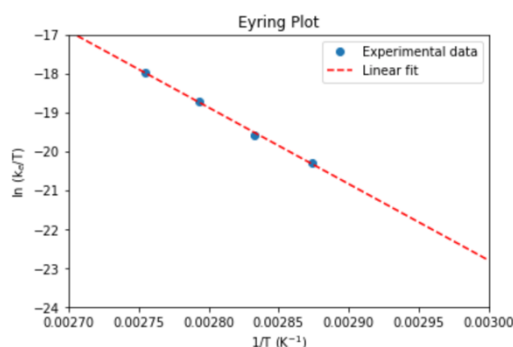By plotting $\ln(k_e/T)$ vs 1/T we obtain the following graph.

Figure S29. Eyring plot for **(P)-Hel-DiDiKTa**.

The linear fit obtained results in the following constants:

a	b	R^2
(-19600±600) K	(36±2)	0.999
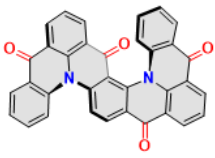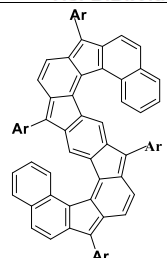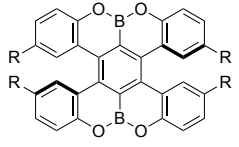
Finally, from the Eyring equation (Equation 12), it is possible to obtain the activation enthalpy and entropy for the enantiomerisation:

$$\Delta H_e^{\ddagger} = -a * R \tag{14}$$

$$\Delta S_e^{\ddagger} = R\left[b - \ln\left(\frac{\kappa\, k_B}{h}\right)\right] \tag{15}$$

The results obtained for **(P)-Hel-DiDiKTa** are shown in Table **S9**, along with the enantiomerisation barriers for other similar helicenes reported in the literature.

Table S10. Activation enthalpy, entropy and Gibbs free energy describing the automerization process obtained for **(P)-Hel-DiDiKTa** (**a**) and other helicenes found in the literature (**b-g**).
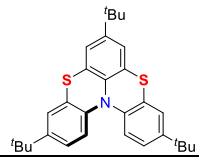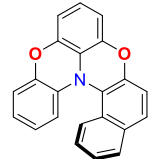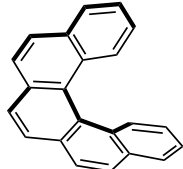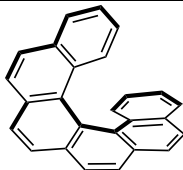
Structure	$\Delta H_e^{\ddagger}$	$\Delta S_e^{\ddagger}$	$\Delta G_e^{\ddagger}$
a Hel-DiDiKTa	39 ± 1 (kcal mol^{-1})	26 ± 1 (cal K^{-1} mol^{-1})	31± 2 (kcal mol^{-1}) (298K) 30± 2 (kcal mol^{-1}) (373K)
b	28.2 (kcal mol^{-1})[37]	49.2 (cal K^{-1}mol^{-1})[37]	14 (kcal mol^{-1}) (298K)
c a) R=H b) R= t-Bu			23 kcal mol^{-1} (298K) (calc)[38] b) 31.8 kcal mol^{-1} (298K) (calc), 29 kcal mol^{-1} (298K) (exp)[38]
d			32.7 kcal mol^{-1} (298K) (calc)[39]
e `			29.0 kcal mol^{-1} (373K)[40]
f	22.9 (kcal mol^{-1})[41]	-4.1 (cal K^{-1} mol^{-1})[41]	24.1 kcal mol^{-1} (298K)
g	33.8 (kcal mol^{-1})[42]	-6.8 (cal K^{-1} mol^{-1})[42]	35.8 kcal mol^{-1} (298K)

Although isomerisation studies for double helicenes are not very common, **(P)-Hel-DiDiKTa** possesses a higher inversion barrier (298 K) than the double S-shaped [6]-helicene reported by Jiang *et al*[37] (**a** versus **b**). This result highlights the high stability of **Hel-DiDiKTa**, the inversion barrier of which also falls in the same range as the double X-shaped [5]helicene **c**. [38]

(P)-Hel-DiDiKTa appears to have a similar enantiomerisation barrier to other bridged phenylamines[39,40] such as **d** and **e**. Moreover, when compared to [5] and [6]-helicene, (*P*)-**Hel-DiDiKTa** has a similar barrier as [6]helicene at room temperature (298 K).[42]

Finally, after obtaining $\Delta H_e^{\ddagger}$ and $\Delta S_e^{\ddagger}$ it is possible to calculate $\Delta G_e^{\ddagger}$ (298 K). Following Equation 16 and 17 , the half-life related to the enantiomerisation process at room temperature can be obtained. [34]

$$k_e(T) = \frac{\kappa\, k_B T}{h} e^{\left(\frac{-\Delta G_e^{\ddagger}(T)}{RT}\right)} \qquad (16)$$

$$t_{\frac{1}{2}}(T) = \frac{\ln 2}{2k_e(T)} \qquad (17)$$

where R is the universal gas constant (R = 8.31446×10^{-3} kJ K^{-1} mol^{-1}), k_B is the Boltzmann constant (1.380662×10^{-23} J K^{-1}), h is Planck's constant, h = 6.626176×10^{-34} J s), k_e is the enantiomerisation rate constant, T is the temperature, $\Delta G_e^{\ddagger}$ is the Gibbs free energy of activation for the enantiomerisation process, and κ is the transmission coefficient.

For **(P)-Hel-DiDiKTa** the half-life obtained is ca. 310 years at room temperature (298 K). Noticeably, this value describes the moment where half of the molecules have been converted to the opposite chirality enantiomer, representing the complete racemisation of the sample and the effective loss of CD signal.

Thermal stability

Stability towards thermal decomposition was studied using thermogravimetric analysis. 1.4 mg of **(rac)-HelDiDiKTa** was placed in a ceramic sample holder and heated at 10 K/min under a 50 mL/min flow of N_2 for 80 mins. The temperature range spanned 30-800 ºC. No decomposition traces were observed in this temperature range, the sample losing only 17% of the mass over the measurement (Figure **S29**).
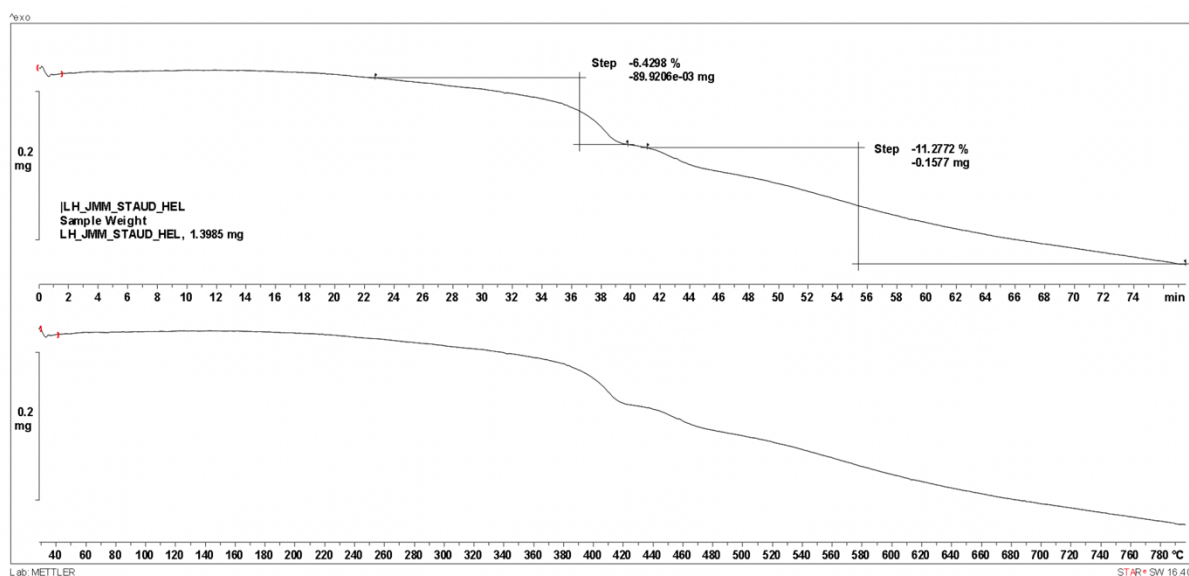
Figure S30. TGA analysis of (*rac*)-**Hel-DiDiKTa**.

References:

1   Y. Yuan, X. Tang, X. Y. Du, Y. Hu, Y. J. Yu, Z. Q. Jiang, L. S. Liao and S. T. Lee, *Adv. Opt. Mater.*, 2019, **7**, 6–11.

2   D. Hall, S. M. Suresh, P. L. dos Santos, E. Duda, S. Bagnich, A. Pershin, P. Rajamalli, D. B. Cordes, A. M. Z. Slawin, D. Beljonne, A. Köhler, I. D. W. Samuel, Y. Olivier and E. Zysman-Colman, *Adv. Opt. Mater.*, 2020, **8**, 1901627.

3   X. Li, Y. Z. Shi, K. Wang, M. Zhang, C. J. Zheng, D. M. Sun, G. Le Dai, X. C. Fan, D. Q. Wang, W. Liu, Y. Q. Li, J. Yu, X. M. Ou, C. Adachi and X. H. Zhang, *ACS Appl. Mater. Interfaces*, 2019, **11**, 13472–13480.

4   D. Sun, S. M. Suresh, D. Hall, M. Zhang, C. Si, D. B. Cordes, A. M. Z. Slawin, Y. Olivier, X. Zhang and E. Zysman-Colman, *Mater. Chem. Front.*, 2020, **4**, 2018–2022.

5   X. Qiu, G. Tian, C. Lin, Y. Pan, X. Ye, B. Wang, D. Ma, D. Hu, Y. Luo and Y. Ma, *Adv. Opt. Mater.*, 2020, **9**, 2001845.

6   S. Zou, C. Peng, S. Yang, Y. Qu, Y. Yu, X. Chen, Z. Jiang and L. Liao, *Org. Lett.*, 2021, **23**, 958–962.

7   H. Min, I. S. Park and T. Yasuda, *Angew. Chemie Int. Ed.*, 2021, **60**, 7643–7648.

8   Y. Tsuchiya, Y. Ishikawa, S. H. Lee, X. K. Chen, J. L. Brédas, H. Nakanotani and C. Adachi, Adv. Opt. Mater., 2021, 9, 2002174.

9   F. Huang, K. Wang, Y. Z. Shi, X. C. Fan, X. Zhang, J. Yu, C. S. Lee and X. H. Zhang, ACS Appl. Mater. Interfaces, 2021, 13, 36089–36097.

10   E. Hamzehpoor and D. F. Perepichka, Angew. Chemie - Int. Ed., 2020, 59, 9977–9981.

11   K. Wang, X.-C. Fan, Y. Tsuchiya, Y.-Z. Shi, M. Tanaka, Z. Lin, Y. Lee, X. Zhang, W. Liu, G. Dai, J.-X. Chen, B. Wu, J. Zhong, Jian-YuYuan, C.-J. Zheng, J. Yu, C.-S. Lee4, C. Adachi and X.-H. Zhang, ChemRxiv. Cambridge Cambridge Open Engag., , DOI:10.26434/chemrxiv.13699057.v1.

12   S.-Y. Yang, S.-N. Zou, F.-C. Kong, X.-J. Liao, Y.-K. Qu, Z.-Q. Feng, Y.-X. Zheng, Z.-Q. Jiang and L.-S. Liao, Chem. Commun., 2021, 57, 11041–11044.

13   *CrystalClear-SM Expert* v2.1. Rigaku Americas. *The Woodlands, Texas,* USA, and Rigaku Corporation. *Tokyo, Japan,* 2015.

14   *CrysAlisPro* v1.171.40.14a. Rigaku Oxford Diffraction, Rigaku Corporation. *Oxford, U.K.,* 2018.

15   G. M. Sheldrick, *Acta Crystallogr., Sect. A.*, 2015, **71**, 3–8.

16   G. M. Sheldrick, *Acta Crystallogr. Sect. C.*, 2015, **71**, 3–8.

17   O. V. Dolomanov, L. J. Bourhis, R. J. Gildea, J. A. K. Howard and H. Puschmann, *J. Appl. Crystallogr.*, 2009, **42**, 339–341.

18   K. Goushi, K. Yoshida, K. Sato and C. Adachi, *Nat. Photonics*, 2012, **6**, 253–258.

19   N. G. Connelly and W. E. Geiger, *Chem. Rev.*, 1996, **96**, 877–910.

20   C. M. Cardona, W. Li, A. E. Kaifer, D. Stockdale and G. C. Bazan, *Adv. Mater.*, 2011, **23**, 2367–2371.

21   F. Zinna, T. Bruhn, C. A. Guido, J. Ahrens, M. Bröring, L. Di Bari and G. Pescitelli, *Chem. - A Eur. J.*, 2016, **22**, 16089–16098.

22   M. J. Frisch, G. W. Trucks, H. B. Schlegel, G. E. Scuseria, M. A. Robb, J. R. Cheeseman, G. Scalmani, V. Barone, G. A. Petersson, H. Nakatsuji, X. Li, M. Caricato, A. V. Marenich, J. Bloino, B. G. Janesko, R. Gomperts, B. Mennucci, H. P. Hratchian, J. V. Ortiz, A. F. Izmaylov, J. L. Sonnenberg, D. Williams-Young, F. Ding, F. Lipparini, F. Egidi, J. Goings, B. Peng, A. Petrone, T. Henderson, D. Ranasinghe, V. G. Zakrzewski, J. Gao, N. Rega, G. Zheng, W. Liang, M. Hada, M. Ehara, K. Toyota, R. Fukuda, J. Hasegawa, M. Ishida, T. Nakajima, Y. Honda, O. Kitao, H. Nakai, T. Vreven, K. Throssell, J. A. Montgomery, Jr., J. E. Peralta, F. Ogliaro, M. J. Bearpark, J. J. Heyd, E. N. Brothers, K. N. Kudin, V. N. Staroverov, T. A. Keith, R. Kobayashi, J. Normand, K. Raghavachari, A. P. Rendell, J. C. Burant, S. S. Iyengar, J. Tomasi, M. Cossi, J. M. Millam, M. Klene, C. Adamo, R. Cammi, J. W. Ochterski, R. L. Martin, K. Morokuma, O. Farkas, J. B. Foresman and D. J. Fox, 2016.

23   S. G. Balasubramani, G. P. Chen, S. Coriani, M. Diedenhofen, M. S. Frank, Y. J. Franzke, F. Furche, R. Grotjahn, M. E. Harding, C. Hättig, A. Hellweg, B. Helmich-Paris, C. Holzer, U. Huniar, M. Kaupp, A. K. Marefat, S. K. Khani, T. Müller, F. Mack, B. D. Nguyen, S. M. Parker, E. Perlt, D. Rappoport, K. Reiter, S. M. R. Roy, G. Schmitz, M. Sierka, E. Tapavicza, D. P. Tew, Artur, C. van Wullen, V. K. Voora, F. Weigend, A. Wodynski and J. M. Yu, *J. Chem. Phys.*, 2020, **152**, 184107.

24   C. Adamo and V. Barone, *J. Chem. Phys.*, 1999, **110**, 6158–6170.

25   T. H. Dunning, *J. Chem. Phys.*, 1989, **90**, 1007–1023.

26   T. Yanai, D. P. Tew and N. C. Handy, *Chem. Phys. Lett.*, 2004, **393**, 51–57.

27   A. D. Becke, *J. Chem. Phys.*, 1993, **98**, 5648–5652.

28   O. A. Vydrov and G. E. Scuseria, *J. Chem. Phys.*, 2006, **125**, 234109.

29   Y. Zhao and D. G. Truhlar, *Theor. Chem. Acc.*, 2008, **120**, 215–241.

30   Gauss View, Version 5. R. Dennington, T. Keith and J. Millam, 2009.

31   G. A. Petersson and M. A. Al-Laham, *J. Chem. Phys.*, 1991, **94**, 6081–6090.

32   J. E. Field, T. J. Hill and D. Venkataraman, *J. Org. Chem.*, 2003, **68**, 6071–6078.

33   H. Kubo, T. Hirose, T. Nakashima, T. Kawai, J. Hasegawa and K. Matsuda, *J. Phys. Chem. Lett.*, 2021, **12**, 686–695.

34   M. Rickhaus, L. Jundt and M. Mayor, *Chimia (Aarau).*, 2016, **70**, 192–202.

35   P. Ravat, *Chem. – A Eur. J.*, 2021, **27**, 3957–3967.

36   P. Osswald and F. Würthner, *J. Am. Chem. Soc.*, 2007, **129**, 14319–14326.

37   Q. Jiang, Y. Han, Y. Zou, H. Phan, L. Yuan, T. S. Herng, J. Ding and C. Chi, *Chem. - A Eur. J.*, 2020, **26**, 15613–15622.

38   T. Katayama, S. Nakatsuka, H. Hirai, N. Yasuda, J. Kumar, T. Kawai and T. Hatakeyama, *J. Am. Chem. Soc.*, 2016, **138**, 5210–5213.

39   B. D. Gliemann, A. G. Petrovic, E. M. Zolnhofer, P. O. Dral, F. Hampel, G. Breitenbruch, P. Schulze, V. Raghavan, K. Meyer, P. L. Polavarapu, N. Berova and M. Kivala, *Chem. – An Asian J.*, 2017, **12**, 31–35.

40   H. Nishimura, K. Tanaka, Y. Morisaki, Y. Chujo, A. Wakamiya and Y. Murata, *J. Org. Chem.*, 2017, **82**, 5242–5249.

41   C. Goedicke and H. Stegemeyer, *Tetrahedron Lett.*, 1970, **11**, 937–940.

42   R. H. Martin and M. J. Marchant, *Tetrahedron Lett.*, 1972, **13**, 3707–3708.